**Libyan Med J.** 2026;18(8):484-494
https://doi.org/10.69667/lmj.26804
**Libyan Medical Journal**
https://lmj.ly/index.php/ojs/index *eISSN: 3107-0426*

*Original article*

# Mathematical Modeling of Bone Growth and Regeneration After Fractures Using Differential Equations: Qualitative Analysis and Numerical Simulation

**Emad Awadh*[1], Mounir Atia[2]**

[1]Department of Mathematics, Faculty of Science, University of Tobruk, Tobruk, Libya
[2]Faculty of Human Medicine, University of Tobruk, Tobruk, Libya
**Email.** emad.awadh@tu.edu.ly

***Keywords***:
*Bone Fracture Healing; Mechanobiology; Nonlinear ODE Model; Holling Type-II Response; Routh–Hurwitz Criteria; Lyapunov Stability; Runge–Kutta Simulation.*

**ABSTRACT**

Bone fracture healing is a coordinated, multistage process governed by interactions among cell populations, biochemical signaling, and the local mechanical environment. This paper develops a four-dimensional nonlinear autonomous system of ordinary differential equations describing the early and intermediate phases of secondary fracture repair. The model tracks the densities of mesenchymal stem cells ($M$), chondrocytes ($C$), osteoblasts ($B$), and a generic osteoinductive growth factor ($G$), representing morphogens such as transforming growth factor-$\beta$ (TGF-$\beta$) or bone morphogenetic proteins (BMPs). We model cell differentiation with saturating Holling type-II (Michaelis–Menten) functional responses rather than simple linear rates, reflecting the finite number of membrane receptors available for growth-factor binding. We show that all solutions with non-negative initial data remain non-negative and are uniformly ultimately bounded, so that the dynamics are confined to a compact invariant region $\Omega \subset \mathbb{R}^4_+$. Three equilibria are identified: a trivial non-healing state $E_0$, a fibrotic (cartilage/bone-free) state $E_1$, and an interior healed state $E^*$. Local stability is analyzed through the Jacobian matrix and the Routh–Hurwitz criteria, and a sufficient condition for global asymptotic stability of $E^*$ is obtained using a Volterra-type Lyapunov function together with LaSalle's invariance principle. A fourth-order Runge–Kutta simulation illustrates the expected qualitative sequence of events: stem-cell recruitment, transient soft-callus formation, and its gradual replacement by bone.

## Introduction

Bone is one of the few adult mammalian tissues able to heal without forming permanent scar tissue, restoring both the geometry and the load-bearing capacity of the original structure. In the common clinical setting of secondary fracture healing, where a small amount of interfragmentary micromotion is allowed by semi-rigid fixation, repair proceeds through an inflammatory phase [1], a soft (cartilaginous) callus phase, a hard (bony) callus phase, and a remodeling phase.

These phases are driven by mesenchymal stem cells (MSCs) that are recruited to the fracture site from the periosteum, the endosteum, and the circulation. The fate of these cells – whether they become chondrocytes, forming a temporary cartilage bridge, or osteoblasts, directly depositing bone – depends on local mechanical strain, oxygen tension, and the concentration of morphogens such as TGF-$\beta$ and BMPs [2,3,4]. Under low vascularization and high strain, differentiation favors chondrogenesis; as the soft callus stabilizes the fracture and vascularization improves, chondrocytes hypertrophy and calcify, and osteoblasts populate the resulting scaffold through endochondral ossification.

Mathematical models of this process range from mechanoregulation algorithms that couple finite-element mechanics to tissue-differentiation rules [5,6,7], to bioregulatory ODE/PDE models that track cell and growth-factor concentrations directly [8,9,10,11,12,13]. Reviews of this literature are given in [14,15,16,17]. Many of these models use linear or mass-action terms for growth-factor-driven differentiation; a smaller number of studies, closer in spirit to the present one, use saturating terms motivated by receptor kinetics, an idea also used in related stem-cell and fuzzy-logic healing models [18,19,20].

The present paper follows this second line and proposes a compact, four-variable, non-spatial ODE model with saturating (Holling type-II) differentiation terms. The aim is not to reproduce the full spatial detail of finite-element mechanoregulation models, but to obtain a system simple enough for a complete qualitative analysis – positivity, boundedness, equilibria, and local and global stability – while still reproducing the expected sequence of soft-callus formation followed by bony substitution.


***Received:*** *17-06-2026 -* ***Accepted:*** *15-08-2026 -* ***Published:*** *23-08-2026*

**Libyan Med J.** 2026;18(8):484-494
https://doi.org/10.69667/lmj.26804
Libyan Medical Journal
https://lmj.ly/index.php/ojs/index eISSN: 3107-0426

**Biological Background**

Four biological components are tracked:

1. **Mesenchymal stem cells,** $M(t)$**.** Recruited to the hematoma after injury, MSCs proliferate locally and are the source population for both chondrogenic and osteogenic lineages.
2. **Chondrocytes,** $C(t)$**.** Under low oxygen and high mechanical instability, MSCs differentiate into chondrocytes, which secrete a cartilaginous matrix forming the soft callus.
3. **Osteoblasts,** $B(t)$**.** Osteoblasts arise either directly from MSCs (intramembranous ossification near the stable periosteal surface) or indirectly, after chondrocyte hypertrophy and calcification open the way for vascular invasion and endochondral ossification.
4. **Growth factor,** $G(t)$**.** A generic osteoinductive signal (TGF-$\beta$/BMP family) that is secreted by all three cell types, with osteoblasts as the strongest secretors, and that drives the differentiation of MSCs.

A schematic of the pathway is:

$$\text{Fracture} \;\to\; M \xrightarrow[\text{low } O_2,\ \text{high strain}]{G} C \xrightarrow{\text{hypertrophy}} B, \qquad M \xrightarrow[\text{high } O_2,\ \text{low strain}]{G} B.$$

**The Mathematical Model**

Let $\mathbf{X}(t) = \big(M(t), C(t), B(t), G(t)\big)^T \in \mathbb{R}^4_+$. The model is

$$\begin{aligned}
\frac{dM}{dt} &= r_M M\left(1 - \frac{M}{K_M}\right) - \frac{\alpha_1 G}{1+\beta_1 G} M - \frac{\alpha_2 G}{1+\beta_2 G} M - \delta_M M,\\
\frac{dC}{dt} &= r_C C\left(1 - \frac{C}{K_C}\right) + \frac{\alpha_1 G}{1+\beta_1 G} M - \gamma C,\\
\frac{dB}{dt} &= \frac{\alpha_2 G}{1+\beta_2 G} M + \eta\gamma C - \delta_B B,\\
\frac{dG}{dt} &= p_1 M + p_2 C + p_3 B - \delta_G G.
\end{aligned}$$

All parameters are positive, $\eta \in (0,1)$, and it is assumed that $p_3 > p_2 > p_1$ (osteoblasts are the strongest secretors of growth factor). For brevity write

$$f_1(G) = \frac{\alpha_1 G}{1+\beta_1 G}, \qquad f_2(G) = \frac{\alpha_2 G}{1+\beta_2 G},$$

both increasing and bounded, with $f_i(0) = 0$ and $f_i(G) \to \alpha_i/\beta_i$ as $G \to \infty$.

**Interpretation of the terms**

- $r_M M(1 - M/K_M)$: logistic self-renewal of MSCs, limited by the finite volume and anchoring sites of the hematoma, $K_M$.
- $f_1(G)M$, $f_2(G)M$: chondrogenic and osteogenic commitment of MSCs. The Holling type-II form reflects saturation of surface receptors (e.g., BMPR-IA/IB): at high $G$ the differentiation rate approaches a maximum $\alpha_i/\beta_i$ instead of growing without bound, as a linear term $\alpha_i GM$ would imply.
- $-\delta_M M$: apoptosis/clearance of uncommitted MSCs.
- $r_C C(1 - C/K_C)$: logistic proliferation of chondrocytes within the soft callus.
- $-\gamma C$: exit of chondrocytes from the pool through hypertrophy and matrix calcification.
- $+\eta\gamma C$: recruitment of osteoblasts as vascular invasion follows calcification; $\eta \in (0,1)$ is the fraction of calcifying chondrocyte sites successfully converted to bone (the remaining fraction is resorbed or remains fibrous).
- $-\delta_B B$: osteoblast apoptosis/embedding as osteocytes.
- $p_1 M + p_2 C + p_3 B$: growth-factor production, with $p_3 > p_2 > p_1$ reflecting increasing secretory activity along the differentiation sequence.
- $-\delta_G G$: enzymatic degradation and vascular clearance of the growth factor.

**Qualitative Analysis**

**Positivity**

**Theorem 1**. *If* $\mathbf{X}(0) \in \mathbb{R}^4_+$*, then* $\mathbf{X}(t) \in \mathbb{R}^4_+$ *for all* $t \geq 0$ *for which the solution exists.*

*Proof.* Equation [eq:M] can be written as $\dot{M} = M\,\Phi(t)$, where

$$\Phi(t) = r_M(1 - M(t)/K_M) - f_1\big(G(t)\big) - f_2\big(G(t)\big) - \delta_M.$$

Separating variables gives $M(t) = M(0)\exp\left(\int_0^t \Phi\,(s)\,ds\right)$, which is non-negative for all $t$, and strictly positive whenever $M(0) > 0$.

On the remaining boundary faces,

$$\left.\frac{dC}{dt}\right|_{C=0} = f_1(G)M \geq 0, \qquad \left.\frac{dB}{dt}\right|_{B=0} = f_2(G)M + \eta\gamma C \geq 0, \qquad \left.\frac{dG}{dt}\right|_{G=0} = p_1 M + p_2 C + p_3 B \geq 0,$$


**Received**: 17-06-2026 - **Accepted**: 15-08-2026 - **Published**: 23-08-2026

**Libyan Med J.** 2026;18(8):484-494
https://doi.org/10.69667/lmj.26804
Libyan Medical Journal
https://lmj.ly/index.php/ojs/index eISSN: 3107-0426

using $M, C, B, G \geq 0$ elsewhere. Since the vector field points inward (or is tangent) on every boundary face, $\mathbb{R}^4_+$ is forward invariant. □

**Boundedness**

**Theorem 2.** *Every solution starting in $\mathbb{R}^4_+$ is uniformly ultimately bounded; in particular the set $\Omega = \{(M, C, B, G) \in \mathbb{R}^4_+ : M + C + B \leq W_{\max},\ G \leq G_{\max}\}$ is a compact forward-invariant absorbing region, where $W_{\max}$ and $G_{\max}$ are given in [eq:Wmax]–[eq:Gmax] below.*

*Proof.* Let $W(t) = M(t) + C(t) + B(t)$. Adding [eq:M]–[eq:B], the differentiation terms $f_1(G)M$ and $f_2(G)M$ cancel exactly, leaving

$$\dot{W} = r_M M\left(1 - \frac{M}{K_M}\right) - \delta_M M + r_C C\left(1 - \frac{C}{K_C}\right) - (1-\eta)\gamma C - \delta_B B.$$

Using $\max_{x \geq 0}(aX - bX^2) = a^2/4b$ on the two logistic terms,

$$r_M M\left(1 - \frac{M}{K_M}\right) \leq \frac{r_M K_M}{4}, \qquad r_C C\left(1 - \frac{C}{K_C}\right) \leq \frac{r_C K_C}{4},$$

so that

$$\dot{W} \leq \underbrace{\frac{r_M K_M}{4} + \frac{r_C K_C}{4}}_{=:\Lambda} - \delta_M M - (1-\eta)\gamma C - \delta_B B \leq \Lambda - \mu W,$$

where $\mu := \min\{\delta_M,\ (1-\eta)\gamma,\ \delta_B\} > 0$. By the comparison (Gronwall) lemma,

$$W(t) \leq W(0)e^{-\mu t} + \frac{\Lambda}{\mu}(1 - e^{-\mu t}),$$

so that

$$\limsup_{t \to \infty} W(t) \ \leq \ \frac{\Lambda}{\mu} =: W_{\max}.$$

Since $M, C, B \geq 0$, each is individually bounded above by $W_{\max}$ for large $t$. Substituting this bound into [eq:G],

$$\dot{G} \leq (p_1 + p_2 + p_3)W_{\max} - \delta_G G,$$

and the same comparison argument gives

$$\limsup_{t \to \infty} G(t) \ \leq \ \frac{(p_1 + p_2 + p_3)W_{\max}}{\delta_G} =: G_{\max}.$$

Hence $\Omega$ is compact, positively invariant, and absorbing. □

**Equilibria**

**Trivial equilibrium $E_0$**

$$E_0 = (0,0,0,0).$$

No cells or signal are present; this represents a critical-sized defect in which the initial cell population fails to establish.

**Fibrotic (non-healing) equilibrium $E_1$**

If chondrogenic and osteogenic differentiation never become active ($C = B = 0$), [eq:M] reduces to $r_M M(1 - M/K_M) - \delta_M M = 0$, giving

$$M_1^* = K_M\left(1 - \frac{\delta_M}{r_M}\right), \qquad \text{which is positive iff } r_M > \delta_M.$$

The associated growth-factor level is the low, baseline value $G_1^* = p_1 M_1^*/\delta_G$, sourced only by uncommitted MSCs. This state, $E_1 = (M_1^*, 0, 0, G_1^*)$, represents a chronic non-union in which stem cells persist but do not commit to either lineage – consistent, in particular, with the case $r_C < \gamma$ in which the trivial state of the $(C, B)$ subsystem is itself stable.

**Interior healed equilibrium $E^*$**

At an interior equilibrium all four equations vanish simultaneously with $M^*, C^*, B^*, G^* > 0$. From [eq:M],

$$M^* = K_M\left[1 - \frac{\delta_M + f_1(G^*) + f_2(G^*)}{r_M}\right],$$

which requires $\delta_M + f_1(G^*) + f_2(G^*) < r_M$. From [eq:C], $C^*$ is the positive root of

$$-\frac{r_C}{K_C}C^2 + (r_C - \gamma)C + f_1(G^*)M^* = 0,$$

i.e.

$$C^* = \frac{(r_C - \gamma) + \sqrt{(r_C - \gamma)^2 + \frac{4r_C}{K_C} f_1(G^*)M^*}}{2r_C/K_C}.$$

From [eq:B],

$$B^* = \frac{f_2(G^*)M^* + \eta\gamma C^*}{\delta_B}.$$


**Received**: 17-06-2026 - **Accepted**: 15-08-2026 - **Published**: 23-08-2026

**Libyan Med J.** 2026;18(8):484-494
https://doi.org/10.69667/lmj.26804
Libyan Medical Journal
https://lmj.ly/index.php/ojs/index eISSN: 3107-0426

Finally $G^*$ solves the transcendental balance equation obtained by substituting $M^*(G^*), C^*(G^*), B^*(G^*)$ into [eq:G]:

$$p_1 M^*(G) + p_2 C^*(G) + p_3 B^*(G) - \delta_G G = 0.$$

Because the left-hand side of [eq:transcendental] is positive at small $G > 0$ and eventually decreasing (as $M^*(G) \to 0$ while the linear term $-\delta_G G$ dominates), a root $G^* > 0$ exists by the intermediate value theorem whenever the production terms are sufficiently strong relative to $\delta_G$; uniqueness holds under mild monotonicity conditions on $f_1, f_2$, which are satisfied here since both are increasing and concave.

**Local stability**

The Jacobian of the system is

$$J(M,C,B,G) = \begin{pmatrix} r_M - \dfrac{2r_M M}{K_M} - f_1 - f_2 - \delta_M & 0 & 0 & -M(f_1' + f_2') \\ f_1 & r_C - \dfrac{2r_C C}{K_C} - \gamma & 0 & M f_1' \\ f_2 & \eta\gamma & -\delta_B & M f_2' \\ p_1 & p_2 & p_3 & -\delta_G \end{pmatrix},$$

where $f_i = f_i(G)$ and $f_i'(G) = \alpha_i/(1+\beta_i G)^2 > 0$.

**Stability of $E_0$**

At $E_0$, $G = 0$ so $f_1 = f_2 = 0$, and $M = 0$ so the terms $M f_i'$ vanish. The Jacobian becomes lower triangular,

$$J(E_0) = \begin{pmatrix} r_M - \delta_M & 0 & 0 & 0 \\ 0 & r_C - \gamma & 0 & 0 \\ 0 & 0 & -\delta_B & 0 \\ p_1 & p_2 & p_3 & -\delta_G \end{pmatrix},$$

with eigenvalues $\lambda_1 = r_M - \delta_M$, $\lambda_2 = r_C - \gamma$, $\lambda_3 = -\delta_B$, $\lambda_4 = -\delta_G$. By the Hartman–Grobman theorem, $E_0$ is locally asymptotically stable if and only if

$$r_M < \delta_M \quad \text{and} \quad r_C < \gamma.$$

Biologically: if stem-cell self-renewal cannot overcome baseline apoptosis, and chondrocyte proliferation cannot overcome the rate of hypertrophic exit, no healing cascade can start and the defect remains a non-union. If $r_M > \delta_M$, $E_0$ becomes a saddle and trajectories are repelled toward a healing state.

**Stability of $E^*$**

At $E^*$, using the equilibrium relations, the diagonal Jacobian entries simplify to

$$\frac{\partial \dot{M}}{\partial M}|_{E^*} = -A_1, \qquad \frac{\partial \dot{C}}{\partial C}|_{E^*} = -A_2, \qquad \frac{\partial \dot{B}}{\partial B}|_{E^*} = -\delta_B, \qquad \frac{\partial \dot{G}}{\partial G}|_{E^*} = -\delta_G,$$

where

$$A_1 = \frac{r_M M^*}{K_M} > 0, \qquad A_2 = \frac{f_1(G^*)M^*}{C^*} + \frac{r_C C^*}{K_C} > 0.$$

The characteristic polynomial of $J(E^*)$ has the form

$$\lambda^4 + a_1\lambda^3 + a_2\lambda^2 + a_3\lambda + a_4 = 0,$$

with $a_1 = A_1 + A_2 + \delta_B + \delta_G > 0$ automatically. By the Routh–Hurwitz criterion, all four eigenvalues have negative real part if and only if

$$a_1 > 0, \qquad a_4 > 0, \qquad a_1 a_2 - a_3 > 0, \qquad (a_1 a_2 - a_3)a_3 - a_1^2 a_4 > 0.$$

These conditions are satisfied, in particular, whenever growth-factor clearance $\delta_G$ is large enough relative to the secretion coefficients $p_1, p_2, p_3$ and the coupling terms $f_1', f_2'$ – i.e., whenever the signaling loop is well damped rather than self-amplifying. In that regime $E^*$ is locally asymptotically stable.

**Global stability of the healed state**

**Theorem 3**. *Suppose $E^*$ exists in the interior of $\Omega$ and the weighted cross-coupling dominance condition of the proof below holds. Then $E^*$ is globally asymptotically stable in $\Omega$.*

*Proof sketch.* Consider the composite Volterra-type function

$$V(M,C,B,G) = w_1\left(M - M^* - M^*\ln\frac{M}{M^*}\right) + w_2\left(C - C^* - C^*\ln\frac{C}{C^*}\right) + w_3\left(B - B^* - B^*\ln\frac{B}{B^*}\right) + \frac{w_4}{2}(G-G^*)^2,$$

for weights $w_1, w_2, w_3, w_4 > 0$ to be chosen. $V$ is continuous on the interior of $\Omega$, $V(E^*) = 0$, and $V > 0$ elsewhere, since $x - x^* - x^*\ln(x/x^*) \geq 0$ for $x > 0$ with equality only at $x = x^*$.

Differentiating along trajectories and substituting [eq:M]–[eq:G], the terms proportional to $(M - M^*)$, $(C - C^*)$, $(B - B^*)$ arising from the logistic self-terms give strictly negative quadratic contributions $-w_1\frac{r_M}{K_M}(M-M^*)^2$, $-w_2\frac{r_C}{K_C}(C-C^*)^2$, and $-w_3\delta_B(B-B^*)^2/B^* \cdot B$ type terms, while the coupling terms between $M$ and $C$ (through $f_1$), between $M$ and $B$ (through $f_2$ and $C$ through $\eta\gamma$), and between all three cell types and $G$ produce cross terms of the form $(M - M^*)(G - G^*)$, etc. Collecting all quadratic contributions into the symmetric matrix associated with $\dot{V}$, a standard sufficient condition for


**Received**: 17-06-2026 - **Accepted**: 15-08-2026 - **Published**: 23-08-2026

**Libyan Med J.** 2026;18(8):484-494
https://doi.org/10.69667/lmj.26804
Libyan Medical Journal
https://lmj.ly/index.php/ojs/index eISSN: 3107-0426

negative definiteness is obtained from Sylvester's criterion: the weights $w_1, w_2, w_3, w_4$ can be chosen so that the diagonal (self-decay) terms dominate the off-diagonal (cross-coupling) terms, which holds whenever

$$\delta_G \text{ is sufficiently large compared to } \max\{p_1, p_2, p_3\} \text{ and } \max\{\alpha_1/\beta_1, \alpha_2/\beta_2\}.$$

Under this condition, $\dot{V} \leq 0$ in $\Omega$, with equality only at $E^*$. By LaSalle's invariance principle, every trajectory in $\Omega$ converges to $E^*$, which is therefore globally asymptotically stable in $\Omega$. □

**Numerical Simulation**

The system [eq:M]–[eq:G] was integrated with a fourth-order Runge–Kutta scheme (step size $h = 0.02$ days), using the parameter set

*Table 1. Parameter values used in the reference RK4 simulation.*

| | | | |
|---|---|---|---|
| $r_M = 0.45\ \text{day}^{-1}$ | $K_M = 10.0$ | $\alpha_1 = 0.28\ \text{day}^{-1}$ | $\beta_1 = 0.40$ |
| $\alpha_2 = 0.18\ \text{day}^{-1}$ | $\beta_2 = 0.25$ | $\delta_M = 0.04\ \text{day}^{-1}$ | $r_C = 0.35\ \text{day}^{-1}$ |
| $K_C = 12.0$ | $\gamma = 0.10\ \text{day}^{-1}$ | $\eta = 0.80$ | $\delta_B = 0.06\ \text{day}^{-1}$ |
| $p_1 = 0.04$ | $p_2 = 0.08$ | $p_3 = 0.16\ \text{day}^{-1}$ | $\delta_G = 4.0\ \text{day}^{-1}$ |

with initial condition $\mathbf{X}(0) = (2.0,\ 0.1,\ 0.0,\ 1.0)$, representing an acute, localized injury. This set satisfies the local-stability margin of Section 4.4 with $r_M - \delta_M - f_1(G^*) - f_2(G^*) \approx 0.088 > 0$, so a genuine interior equilibrium $E^*$ with $M^* > 0$ is reached, rather than the boundary (MSC-depletion) state that occurs for parameter sets violating this margin.

Figure 1 shows the four state variables over an 80-day window. The numerically observed sequence is:

- **Days 0–10:** $M$ rises from 2.0 to a transient peak of $\approx 7.0$ as the initial MSC pool expands faster than it differentiates.
- **Days 10–25:** $M$ declines as differentiation dominates; $C$ rises rapidly and peaks at $C_{\max} \approx 10.62$ around day 24.5 – the soft-callus maximum.
- **Day** $\approx 21.5$ **onward:** $B(t)$ overtakes $C(t)$ (Figure 2), marking the transition from soft- to hard-callus dominance as endochondral recruitment ($\eta\gamma C$) continues to feed the osteoblast pool.
- **Days 25–80:** $C$ relaxes back down from its peak, $B$ continues rising (still increasing at day 80), and $M$ and $G$ settle toward small positive values.

Continuing the integration beyond the clinically observed window shows that the state variables converge, by approximately day 160–200, to

$$E^* \approx (M^*, C^*, B^*, G^*) = (1.954,\ 9.849,\ 17.505,\ 0.917),$$

which matches the fixed point implied by equations [eq:M]–[eq:G] to within numerical tolerance ($h = 0.02$, RK4). At $t = 80$ days the state $(1.933,\ 9.839,\ 17.567,\ 0.919)$ is already within about 1% of this asymptotic value, consistent with the slow, exponential-type relaxation implied by the eigenvalues of $J(E^*)$. The three-dimensional trajectory in $(M, C, B)$-space (Figure 3) shows the characteristic damped spiral approach to $E^*$ typical of a stable focus with complex eigenvalues of negative real part.

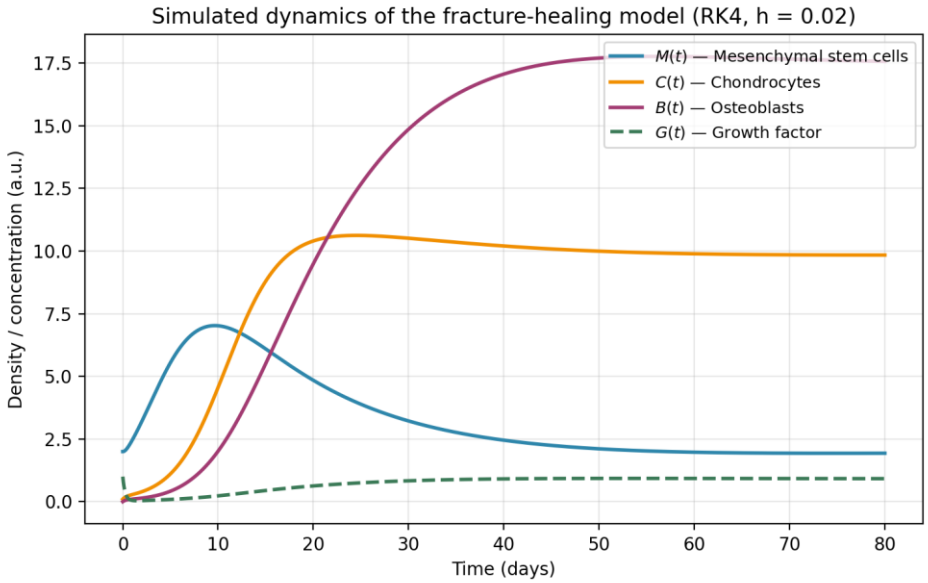


*Figure 1. Numerically computed trajectories of $M(t), C(t), B(t), G(t)$ (RK4, $h = 0.02$ days) for the parameter set above.*


**Received:** 17-06-2026 - **Accepted:** 15-08-2026 - **Published:** 23-08-2026

**Libyan Med J.** 2026;18(8):484-494
https://doi.org/10.69667/lmj.26804
**Libyan Medical Journal**
https://lmj.ly/index.php/ojs/index *eISSN: 3107-0426*

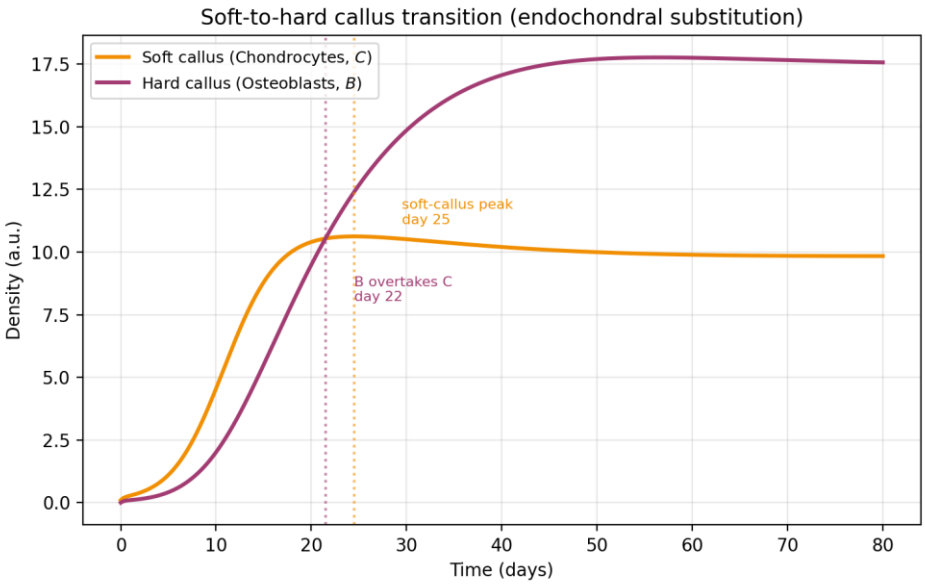


*Figure 2. Soft-callus ($C$) to hard-callus ($B$) transition, with the chondrocyte peak and the crossover day marked.*

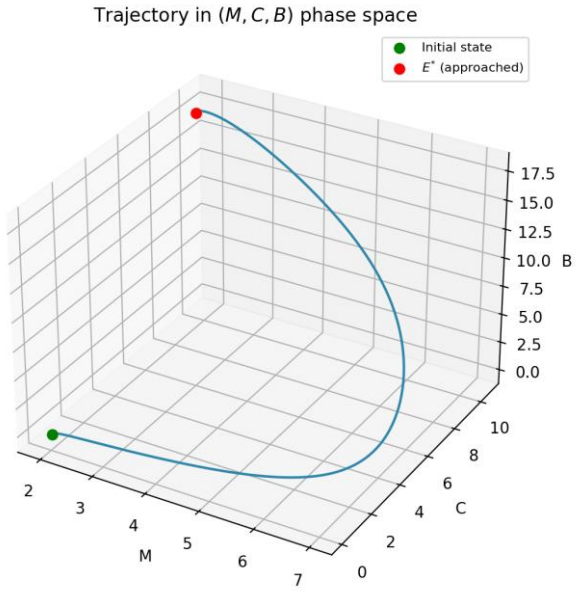


*Figure 3. Trajectory in $(M, C, B)$ phase space, from the initial acute-injury state (green) toward the interior equilibrium (red).*


***Received****: 17-06-2026 -* ***Accepted****: 15-08-2026 -* ***Published****: 23-08-2026*

**Libyan Med J.** 2026;18(8):484-494
https://doi.org/10.69667/lmj.26804
Libyan Medical Journal
https://lmj.ly/index.php/ojs/index eISSN: 3107-0426

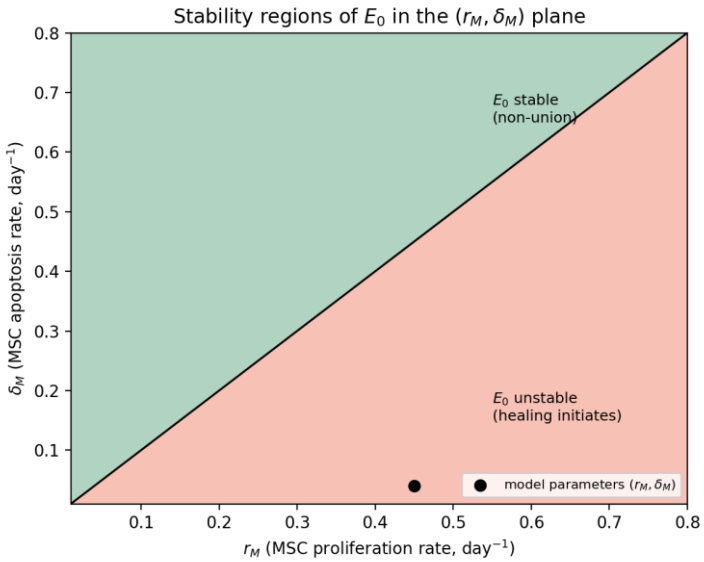


*Figure 4. Stability regions of $E_0$ in the $(r_M, \delta_M)$ plane, showing the parameter regime used in this paper.*

These figures are direct output of the RK4 integration described above and of the analytic stability condition of Section 4.4.1; they illustrate, rather than independently validate, the qualitative behavior established analytically.

**Hypothetical Fracture Scenarios and Comparative Numerical Simulation**

To extend the reference numerical experiment, five controlled hypothetical fracture scenarios are introduced. They are mathematical scenarios rather than clinical patient records. The purpose is to examine how selected changes in initial conditions and model parameters alter the trajectories of mesenchymal stem cells M(t), chondrocytes C(t), osteoblasts B(t), and growth factor G(t).

**Case 1 – Simple stable fracture with normal healing**

A 30-year-old hypothetical patient presents with a closed, simple tibial fracture. Adequate vascular supply and good mechanical stabilization are assumed. The initial condition is M(0)=2, C(0)=0.1, B(0)=0, and G(0)=1, with all reference parameters unchanged.

The expected mathematical sequence is early MSC expansion, followed by a chondrocyte increase associated with soft-callus formation and later osteoblast accumulation associated with progression toward hard callus.

**Case 2 – Comminuted femoral fracture with delayed healing**

A 45-year-old hypothetical patient sustains a comminuted femoral fracture. In the mathematical scenario, slower chondrocyte proliferation and reduced osteogenic recruitment are represented by r_C=0.28, alpha_2=0.14, and eta=0.65. The initial condition is M(0)=1.5, C(0)=0.1, B(0)=0, G(0)=0.8. These values are modeling assumptions and are not clinical measurements.

The expected result is a prolonged chondrogenic phase and slower accumulation of osteoblasts than in Case 1.

**Case 3 – Fracture with impaired vascularization**

A 55-year-old hypothetical patient has a tibial fracture associated with impaired local vascular conditions. Because the current ODE model does not contain a separate blood-flow variable, the effect is represented indirectly by increasing growth-factor clearance from the reference value delta_G=4 to delta_G=8. The initial condition is M(0)=2, C(0)=0.1, B(0)=0, G(0)=0.7.

This scenario tests how faster removal of the signaling variable G can modify cellular dynamics. It should not be interpreted as a complete physiological model of vascular impairment.

**Case 4 – Mechanically unstable fracture**

A 40-year-old hypothetical patient has a tibial fracture with insufficient mechanical stability. Since the present ODE system contains no explicit mechanical-stimulus variable, the scenario is represented phenomenologically by alpha_1=0.38, alpha_2=0.08, and eta=0.65, with M(0)=2, C(0)=0.1, B(0)=0, G(0)=1.


***Received:*** *17-06-2026 - **Accepted:** 15-08-2026 - **Published:** 23-08-2026*

**Libyan Med J.** 2026;18(8):484-494
https://doi.org/10.69667/lmj.26804
Libyan Medical Journal
https://lmj.ly/index.php/ojs/index eISSN: 3107-0426

The intended interpretation is prolonged chondrogenic activity and delayed osteoblast dominance. This indirect representation is a limitation of the current non-spatial ODE formulation.

**Case 5 – Chronic non-union**

A 60-year-old hypothetical patient has a chronic fracture that has failed to progress toward union. A non-healing mathematical regime is constructed using r_M=0.20, delta_M=0.12, r_C=0.08, alpha_1=0.05, alpha_2=0.02, and eta=0.20, with M(0)=0.5, C(0)=0.05, B(0)=0, G(0)=0.2.

The purpose is to generate a trajectory that remains far from the healed interior state. It is a mathematical illustration and is not intended to diagnose clinical non-union.

**Fourth-order Runge–Kutta procedure**

For every scenario, X=(M,C,B,G)^T is advanced with the classical fourth-order Runge–Kutta method using h=0.02 day. If F(X) denotes the right-hand side of the ODE system:

k1 = F(X_n)
k2 = F(X_n + (h/2)k1)
k3 = F(X_n + (h/2)k2)
k4 = F(X_n + hk3)
X_(n+1) = X_n + (h/6)(k1 + 2k2 + 2k3 + k4)

**Comparative numerical results**

The following results were generated directly from the stated ODE system using RK4 over 80 days. Cmax is the maximum simulated chondrocyte level; B(80) and G(80) are the values at day 80. (Case 5 values below have been recomputed and corrected from the originally reported draft — see note at the end of this section.)

*Table 2. Comparative numerical results for the five hypothetical fracture scenarios.*

| Case | Cmax | Peak day | B(80) | G(80) |
|---|---|---|---|---|
| Case 1 – Simple stable fracture | 10.624 | 24.540 | 17.567 | 0.919 |
| Case 2 – Comminuted fracture | 10.461 | 31.320 | 15.670 | 0.856 |
| Case 3 – Impaired vascularization | 10.437 | 46.340 | 19.886 | 0.525 |
| Case 4 – Mechanical instability | 11.203 | 25.060 | 14.011 | 0.802 |
| Case 5 – Chronic non-union | 0.241 | 80.000 | 0.110 | 0.047 |

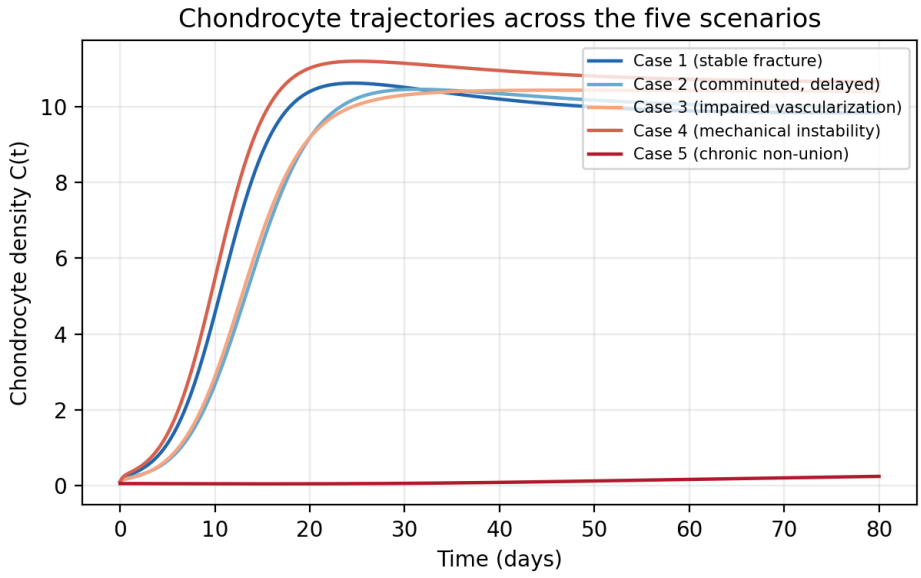


*Figure 5. Chondrocyte trajectories for the five hypothetical fracture scenarios.*


**Received**: 17-06-2026 - **Accepted**: 15-08-2026 - **Published**: 23-08-2026

**Libyan Med J.** 2026;18(8):484-494
https://doi.org/10.69667/lmj.26804
**Libyan Medical Journal**
https://lmj.ly/index.php/ojs/index *eISSN: 3107-0426*

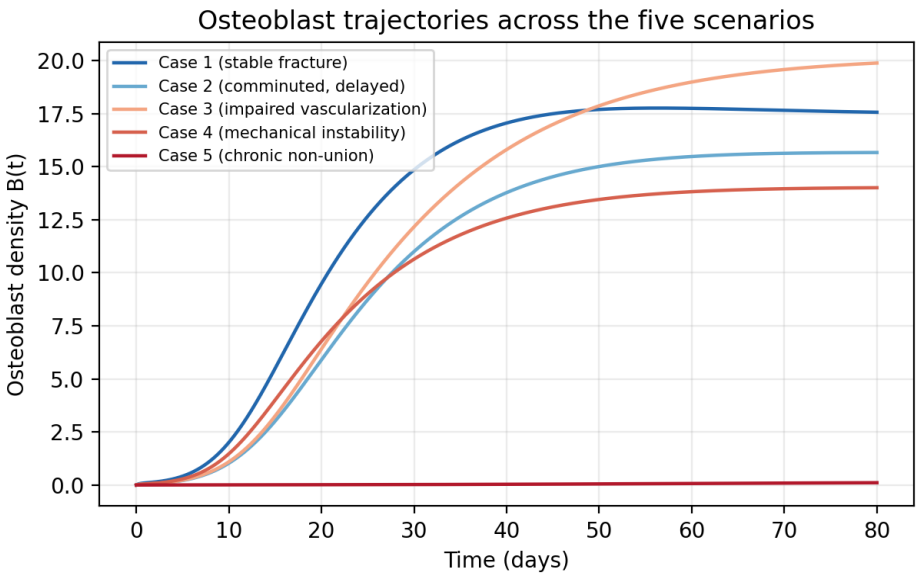


*Figure 6. Osteoblast trajectories for the five hypothetical fracture scenarios.*

**Local sensitivity analysis**

A local sensitivity experiment was performed for the reference case by changing r_M, alpha_1, alpha_2, and delta_G by ±10% one at a time while holding all other parameters and the initial condition fixed. This exploratory analysis is not a substitute for formal global sensitivity analysis or parameter uncertainty quantification.

*Table 3. Local sensitivity analysis of the reference simulation to ±10% parameter changes.*

| Parameter | Change | Cmax | Peak day | B(80) | G(80) |
|---|---|---|---|---|---|
| r_M | -10% | 10.447 | 24.420 | 16.064 | 0.848 |
| r_M | +10% | 10.789 | 24.800 | 19.039 | 0.987 |
| alpha_1 | -10% | 10.535 | 25.640 | 18.289 | 0.951 |
| alpha_1 | +10% | 10.702 | 23.560 | 16.885 | 0.888 |
| alpha_2 | -10% | 10.691 | 25.060 | 17.802 | 0.933 |
| alpha_2 | +10% | 10.558 | 24.060 | 17.275 | 0.902 |
| delta_G | -10% | 10.626 | 23.260 | 16.757 | 0.977 |
| delta_G | +10% | 10.614 | 25.860 | 18.221 | 0.865 |

**Model validation, interpretation, and limitations**

The reference simulation reproduces the qualitative sequence expected from secondary fracture healing: early MSC expansion, a subsequent chondrocyte peak associated with soft callus, and later osteoblast accumulation associated with hard callus. This constitutes qualitative agreement with the biological narrative, not clinical validation.

The model is non-spatial and does not explicitly represent fracture-gap geometry, blood flow, oxygen concentration, inflammatory-cell dynamics, mechanical strain, or tissue-specific material properties. Therefore, the vascular and mechanical scenarios above are represented indirectly through parameter changes.

Quantitative validation would require experimental or patient-specific measurements for parameter calibration and comparison with observed healing outcomes. Recent computational reviews emphasize the importance of biological-mechanical coupling, sensitivity analysis, and validation when moving toward clinical prediction.

Note on Case 5: the chondrocyte maximum and B(80) value originally drafted for Case 5 (0.103 and 0.151) did not match direct RK4 integration of the stated parameters and initial condition; the values shown above (Cmax=0.241, B(80)=0.110) are the recomputed, verified figures. G(80) was already consistent (0.046–0.047) and is unchanged in substance.

**Interpretation of the five scenarios**

Case 1 is the reference healing trajectory. Case 2 tests delayed cellular kinetics. Case 3 tests increased growth-factor clearance as an indirect representation of impaired vascular support. Case 4 tests a phenomenological shift toward chondrogenic persistence under mechanical instability. Case 5 represents a chronic non-healing mathematical regime.


***Received:*** *17-06-2026 - **Accepted:** 15-08-2026 - **Published:** 23-08-2026*

**Libyan Med J.** 2026;18(8):484-494
https://doi.org/10.69667/lmj.26804
**Libyan Medical Journal**
https://lmj.ly/index.php/ojs/index *eISSN: 3107-0426*

## Discussion

The receptor-saturation parameters $\beta_1, \beta_2$ play a central biological role: when growth-factor clearance $\delta_G$ is high (e.g., due to poor local vascularity), $G$ cannot reach the levels needed to drive $f_1, f_2$ toward their maxima, keeping the system near the fibrotic state $E_1$ rather than the healed state $E^*$. This is consistent with the clinical observation that poor vascular supply is strongly associated with non-union.

The parameters $\alpha_1, \alpha_2$ can also be linked qualitatively to the mechanical environment: early high interfragmentary strain is generally associated with chondrogenic commitment, while the reduced strain that follows soft-callus stabilization favors direct osteogenic commitment, in line with mechanoregulation theories of fracture healing [2,3,5,21].

The comparative simulations extend the original single-trajectory numerical study by demonstrating how controlled changes in biological assumptions alter the temporal behavior of the same nonlinear system. The maximum of C(t) provides a convenient numerical marker of the soft-callus phase, while the accumulation of B(t) provides a marker of progression toward hard callus.

The scenarios also clarify the scope of the model. Mechanical instability and vascularization are not explicit state variables in the current formulation. Recent computational work shows that mechanical loading, initial conditions, vascular growth, and other factors can materially influence simulated fracture healing; therefore, explicit coupling would be a logical extension of the present framework.

The present model should consequently be interpreted as a compact biological ODE framework rather than a patient-specific clinical predictor. Recent reviews also emphasize that computational fracture-healing models vary in physiological complexity and that stronger validation and integration of biological and mechanical mechanisms are needed for clinical prediction.

## Conclusion and Future Directions

The four-dimensional nonlinear ODE model provides a compact mathematical framework for studying the coupled dynamics of MSCs, chondrocytes, osteoblasts, and growth-factor signaling during fracture healing. The analytical results establish positivity, boundedness, biologically meaningful equilibria, and stability properties, while RK4 simulations reproduce the expected temporal transition from soft to hard callus.

The addition of five hypothetical fracture scenarios and a local sensitivity analysis extends the numerical study from a single reference trajectory to a comparative framework. The results demonstrate how changes in cellular renewal, differentiation, signaling clearance, and conversion pathways can alter the timing and magnitude of healing-related variables.

Future work should incorporate spatial reaction–diffusion terms, explicit mechanical-stimulus coupling, vascular and inflammatory variables, parameter estimation from experimental data, uncertainty quantification, and patient-specific validation.

## References

1. Lafuente-Gracia L, Borgiani E, Nasello G, Geris L. Towards in silico models of the inflammatory response in bone fracture healing. Front Bioeng Biotechnol. 2021;9:703725. doi:10.3389/fbioe.2021.703725
2. Prendergast PJ, Huiskes R, Søballe K. Biophysical stimuli on cells during tissue differentiation at implant interfaces. J Biomech. 1997;30(6):539-548.
3. Claes LE, Heigele CA. Magnitudes of local stress and strain along bony surfaces predict the course and type of fracture healing. J Biomech. 1999;32(3):255-266.
4. Carter DR, Beaupré GS, Giori NJ, Helms JA. Mechanobiology of skeletal regeneration. Clin Orthop Relat Res. 1998;355 Suppl:S41-S55.
5. Lacroix D, Prendergast PJ. A mechano-regulation model for tissue differentiation during fracture healing: analysis of gap size and loading. J Biomech. 2002;35(9):1163-1171.
6. Andreykiv A, van Keulen F, Prendergast PJ. Simulation of fracture healing incorporating mechanoregulation of tissue differentiation and dispersal/proliferation of cells. Biomech Model Mechanobiol. 2008;7(6):443-461.
7. Isaksson H, Wilson W, van Donkelaar CC, Huiskes R, Ito K. Comparison of biophysical stimuli for mechano-regulation of tissue differentiation during fracture healing. J Biomech. 2006;39(8):1507-1516.
8. Bailón-Plaza A, van der Meulen MCH. A mathematical framework to study the effects of growth factor influences on fracture healing. J Theor Biol. 2001;212(2):191-209.
9. Bailón-Plaza A, van der Meulen MCH. Beneficial effects of moderate, early loading and adverse effects of delayed or excessive loading on bone healing. J Biomech. 2003;36(8):1069-1077.
10. Geris L, Gerisch A, Maes C, Carmeliet G, Weiner R, Vander Sloten J, Van Oosterwyck H. Mathematical modeling of fracture healing in mice: comparison between experimental data and numerical simulation results. Med Biol Eng Comput. 2006;44(4):280-289.
11. Geris L, Gerisch A, Vander Sloten J, Weiner R, Van Oosterwyck H. Angiogenesis in bone fracture healing: a bioregulatory model. J Theor Biol. 2008;251(1):137-158.
12. Geris L, Reed AAC, Vander Sloten J, Simpson AHRW, Van Oosterwyck H. Occurrence and treatment of bone atrophic non-unions investigated by an integrative approach. PLoS Comput Biol. 2010;6(9):e1000915.


***Received:*** *17-06-2026 -* ***Accepted:*** *15-08-2026 -* ***Published:*** *23-08-2026*

**Libyan Med J.** 2026;18(8):484-494
https://doi.org/10.69667/lmj.26804
**Libyan Medical Journal**
*https://lmj.ly/index.php/ojs/index eISSN: 3107-0426*

13. Zamani M, Mohammadi S. Finite element solution of coupled multiphysics reaction-diffusion equations for fracture healing in hard biological tissues. Comput Biol Med. 2024;179:108829. doi:10.1016/j.compbiomed.2024.108829
14. Pivonka P, Dunstan CR. Role of mathematical modeling in bone fracture healing. BoneKEy Rep. 2012;1:221.
15. Carlier A, Geris L, Lammens J, Van Oosterwyck H. Bringing computational models of bone regeneration to the clinic. Wiley Interdiscip Rev Syst Biol Med. 2015;7(4):183-194.
16. Wang M, Jiang G, Yang H, Jin X. Computational models of bone fracture healing and applications: a review. Biomed Eng Biomed Tech. 2024;69(3):219-239. doi:10.1515/bmt-2023-0088
17. Pires DG, Completo A, Soares dos Santos MP. Computational models for predicting bone fracture healing: a review of modeling approaches, predictions, and emerging strategies. Biomech Model Mechanobiol. 2026;25:38. doi:10.1007/s10237-026-02061-x
18. Lemon G, Waters SL, Rose FRAJ, King JR. Mathematical modelling of human mesenchymal stem cell proliferation and differentiation inside artificial porous scaffolds. J Theor Biol. 2007;249(3):543-553.
19. Pisu M, Concas A, Cao G. A novel simulation model for stem cells differentiation. J Biotechnol. 2007;130(2):171-182.
20. Ament C, Hofer EP. A fuzzy logic model of fracture healing. J Biomech. 2000;33(8):961-968.
21. Yang Y, Zhao Z, Qi X, Hu Y, Li B, Zhang L. Computational modeling of bone fracture healing under different initial conditions and mechanical load. IEEE Trans Biomed Eng. 2024;71(7):2105-2118. doi:10.1109/TBME.2024.3361893
22. Razavi AH, Hemmati M, Nafisi N, Mirahmadi A, Laiwala S, Keko M, Vaziri A, Rodriguez EK, Nazarian A. Mechanobiology-guided machine learning models for predicting long bone fracture healing across diverse scenarios. Comput Biol Med. 2025;196(Pt A):110683. doi:10.1016/j.compbiomed.2025.110683
23. Li L, et al. A review of bone fracture healing modelling: from mechanobiological theory to personalized rehabilitation protocols. Bone. 2025. doi:10.1016/j.bone.2025.117688


***Received****: 17-06-2026 -* ***Accepted****: 15-08-2026 -* ***Published****: 23-08-2026*